Vibration–Based Statistical Damage Detection For Scale Wind Turbine Blades Under Varying Environmental Conditions

Ana Gómez González, Spilios D. Fassois

Stochastic Mechanical Systems & Automation (SMSA) Laboratory
University of Patras, GR 265 04 Patras, Greece
anagomez@upatras.gr, fassois@mech.upatras.gr
www.smsa.upatras.gr

Abstract

The problem of damage detection for wind turbine blades under varying environmental conditions and different damage scenarios is considered. A lab–scale blade subject to two levels of damage and conditions is considered under conditions including sprayed water (simulating rain) and temperatures in the range $[-20,20]$°C. A vibration–based statistical time series type methodology employing Principal Component Analysis (PCA) is postulated. Two different versions are employed: the first is an output–only scheme based on the vibration response Power Spectral Density (PSD), and the second is an input–output scheme based on the input–output Frequency Response Function (FRF). Detection is based on principal components selected to be independent of environmental conditions, but still sensitive to damage. A single vibration acceleration response is used in the study. The damage detection results are slightly better for the FRF based version, compared to the PSD based one, with detection rates over 96.5% and false alarm rates below 1.5%.

1 Introduction

Structural damage detection is of primary importance in mechanical, aerospace and civil engineering. When dealing with structural damage detection methods, it is very important to account for uncertainties in the measurements and varying environmental and/or operating conditions. The fact of not taking them into consideration is an important limitation of many existing methods, which is restricting their applicability. In order to avoid such a situation, methods able to account for environmental and/or operational variability are needed. This problem is often referred to as the data normalization problem (see [1] for a detailed review of such methods). In general a big bank of data under normal condition (and varying environmental and operational conditions) is needed. Mainly two classes of normalization methods can be used.

When the environmental and/or operational conditions are measurable and available, a first class of methods is based on directly modeling the dependence of the environmental and/or operating conditions on the dynamics. Within this class two further approaches may be distinguished. The first is a *multi–model* approach in which a model is obtained for each specific condition, and then the models are linked via different techniques. Some establish relationships between modal parameters (such as eigenfrequencies) and temperature by means of correction formulae [2], ARX models [3] or linear filters [4]. Some others, link the obtained model parameters to temperature via regression or interpolation techniques [5]. In [6] clustering for different environmental conditions is introduced. The main drawback of this multi–model approach is that a large number of separate models are obtained, not taking into account their potential interrelations. To overcome this drawback, *global models* may be introduced. In [7] two such methods are described. The first is based on a Constant Coefficient Pooled (CCP) model which provides an averaged description and consequently limited information of dependence on environmental factors (in this case temperature). The second is based on Functionally Pooled (FP) models, where this dependence is modeled in a functional form. This latter method offers a more compact description of the dynamics, improved numerical robustness and estimation accuracy, as well as better overall performance.

A second class of methods, that do not need the specific environmental and/or operational conditions to be available, is based on obtaining a characteristic quantity that is sensitive to damage but insensitive to changes in the environmental and/or operating conditions. A number of methods may be used for obtaining such a quantity, including a simple *outlier analysis* [8]; *Principal Component Analysis* (PCA) [8, 9] which searches for orthogonal directions with maximum variability, and removes the first ones, in the hope that damage will affect (also) some of the remaining components not affected by environmental and operational variation (in [8] these first two techniques have reportedly not been very successful); *factor analysis* [10], which tries to identify a linear subspace in which the environmental effects lie and then project the measured data in the orthogonal subspace; *averaging techniques* [11], based on the null–space method, an averaged sample Hankel matrix is used that already accounts for all the normal condition of the structure; *cointegration* [12], which tries to find (and eliminate) common trends on the normal condition data that are often caused by environmental or operational variations, and so on.

An important field of application of damage detection techniques in which the inclusion of varying environmental and operating conditions is crucial, is that of renewable energy structures, such as wind turbines. For wind turbines these varying conditions may be due to weather (temperature, humidity), wind speed, varying rotational speed, and so forth. A change in a specific condition may often lead to a false alarm. The increase in the size of wind turbines, in an effort to capture as much wind energy as possible, has led to increasingly larger wind turbine blades. On the other hand, turbine blades are subject to damage, and this may even cause damage to the tower [13, 14]. The need to continuously monitor the health state of these structures is thus evident, as visual inspection is not a viable option. Previous studies [15] have analyzed changes in modal frequencies under different damage scenarios of a laboratory scale wind turbine blade, reaching the conclusion that the first seven modes may be sufficient to indicate damage. Yet no actual damage detection is performed. In another study [16], fatigue tests on full size blades have been performed, using the results to validate different damage detection methods, such as acoustic emission, virtual forces, or time-frequency analysis. In [13] a 1–meter–long section of a wind turbine blade has been analyzed via different vibration based methods: Lamb wave propagation, frequency response analysis, and time series methods. The damage was simulated by adding a piece of putty on the surface. In all methods the damage index (characteristic quantity) used has been obtained from cross-correlations between a baseline signal and a corresponding signal from a current (healthy or damaged) state, while slightly varying conditions are considered (position of the blade section on the table). The differences due to damage in this case are larger than those due to the considered variations, and detection is performed by comparing to a single "healthy" baseline case with good overall results (of course with dependence on the damage location).

In the present study a vibration–based statistical time series type methodology for damage detection under varying environmental and/or operating conditions is postulated and applied to damage detection in laboratory–scale wind turbine blades. The environmental conditions are varying due to the potential presence of sprayed water (simulating rain) on the blade and temperatures varying in the range of $[-20, 20]$°C. The postulated methodology belongs to the second of the described classes. This is a companion paper to our work in [17] and extends it in the sense that it includes, along with the Power Spectral Density (PSD, output–only) based version presented there, the Frequency Response Function (FRF, input–output) based version. One single vibration response, together with the input in the FRF based version, is used at a time. In both papers the methodology is based on Principal Component Analysis (PCA), with an additional difference being the way in which the specific components are selected for damage detection.

2 The experimental set-up

The lab–scale wind turbine blade (length 0.77 m, maximum width 0.135 m, mass 0.646 kg) is shown in the drawing of Figure 1(a). It is placed in a freezer and clamped (by means of 3 bolts – torque of 5 N·m) on one end on a steel base in a cantilever position and excited by a shaker, see Figure 1(b). The experiments are carried out under quasi–static thermal conditions, with the temperature obtained from a digital thermometer with a K–type bead thermocouple attached near the clamp. The study focuses on the temperature range $[-20, 20]$°C. Water spraying is used for simulating rainy conditions.

Two levels of damage are used: The first one (D1) is semicircular damage at the trailing edge of the blade with a radius of 2.5 mm (Figure 2(a)). The second (D2) is based on the previous by enlarging the hole. The total length now is 1.5 cm, whereas the depth remains at 2.5 mm (Figure 2(b)).

Damage detection is based on a *single* selected vibration acceleration response signal at a time. The ex-

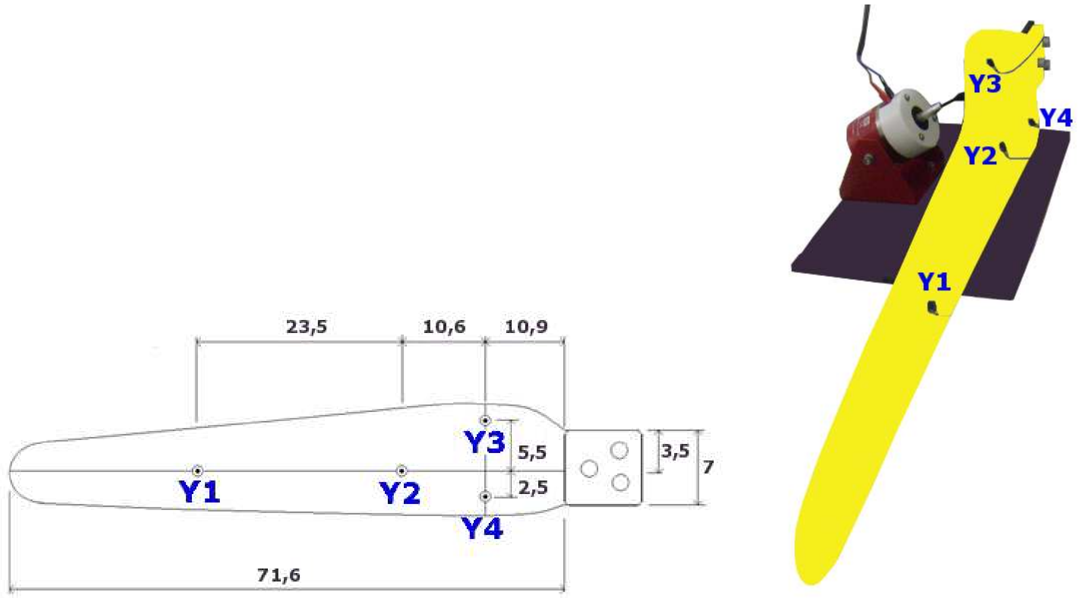

(a) (b)

Figure 1: (a) Drawing of the lab-scale blade showing the acceleration measurement positions (Y1–Y4; distances in cm), (b) photo of the experimental set-up showing the clamping, the shaker, and the acceleration measurement positions.

Blade Health State	*Temperature step – Number of cases (Temp. range* $-20..20°C$*)*	*Number of experiments (at each temperature)*		*Total number of experiments (data records)*			
		Baseline	*Inspection*	*Baseline*		*Inspection*	
Healthy	Step 2°C – 21 cases	5	35	105	**160**	735	**1 120**
Healthy with water	Step 4°C – 11 cases	5	35	55		385	
Damage 1	Step 4°C – 11 cases	5	35	55	**55**	385	**385**
Damage 2	Step 2°C – 21 cases	5	35	105	**160**	735	**1 120**
Damage 2 with water	Step 4°C – 11 cases	5	35	55		385	
Sampling frequency $f_s = 5\ 120$ Hz Signal bandwidth $20 - 2\ 000$ Hz Signal length $N = 32\ 768$ samples (6.4 s)							

Table 1: Overview of the experiments

citation is random stationary (bandwidth of $20 - 2\ 000$ Hz; details in Figure 3) and is measured by means of an impedance head (PCB M288D01, sensitivity 98.41 mV/lb), it will be used in the FRF based version of the method. Four lightweight accelerometers are used to measure the vibration response at Points Y1, Y2, Y3 and Y4. All signals are collected by means of two SigLab modules at a sampling frequency of $f_s = 5\ 120$ Hz. Following sample mean subtraction, each signal is normalized to unit sample variance. An overview of the experiments carried out is available in Table 1.

3 The damage detection methodology

The damage detection methodology is based on changes in the Power Spectral Density (PSD) of a *single* vibration response signal (the output–only version) or the Frequency Response Function (FRF) of a *single* vibration response signal with respect to the input (the input–output version) [18].

For a given measured vibration response signal $y[t]$, and its corresponding input $x[t]$, $t = 1, \ldots, N$ (with sample mean subtracted and normalized to unity sample variance), the Welch PSD and FRF estimates are used [18] (MATLAB functions *pwelch.m* for the PSD and *tfestimate* for the FRF). Namely, the Welch PSD estimate

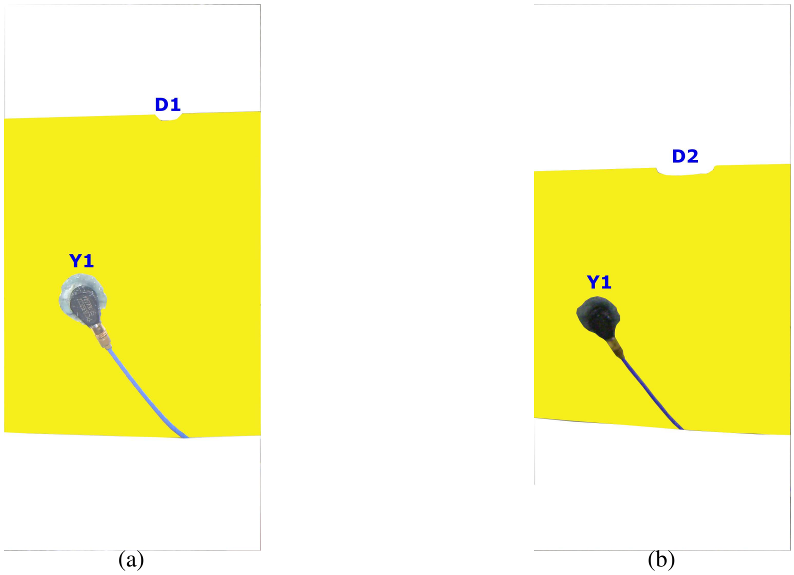

Figure 2: Detail of the considered damages: (a) damage D1 (small), (b) damage D2 (large).

for the output sequence is given by:

$$\widehat{S}_{yy}(\omega) = \frac{1}{K}\sum_{i=1}^{K} Y_L^{(i)}(j\omega)\cdot Y_L^{(i)}(-j\omega), \text{ with } Y_L^{(i)}(j\omega) = \frac{1}{\sqrt{L}}\sum_{t=1}^{L} a[t]y^{(i)}[t]e^{-j\omega t T_s}, \tag{1}$$

where $\omega \in [0, 2\pi/T_s]$ stands for frequency in rad/s, j for the imaginary unit, K for the number of segments (each of length L) and $a[t]$ the selected time window. The superscript (i) indicates a specific segment of the signal. Analogously the Welch PSD estimate for the input sequence $\widehat{S}_{xx}(\omega)$ is defined. The Welch Cross Power Spectral Density (CPSD) estimate between the input and the output is given by:

$$\widehat{S}_{yx}(j\omega) = \frac{1}{K}\sum_{i=1}^{K} Y_L^{(i)}(j\omega)\cdot X_L^{(i)}(-j\omega), \text{ with } X_L^{(i)}(j\omega) = \frac{1}{\sqrt{L}}\sum_{t=1}^{L} a[t]x^{(i)}[t]e^{-j\omega t T_s}. \tag{2}$$

Finally the Welch FRF estimate is obtained as:

$$\widehat{H}(j\omega) = \widehat{S}_{yx}(j\omega)/\widehat{S}_{xx}(\omega). \tag{3}$$

In the following $\boldsymbol{\theta} \in \mathbb{R}^n$ represents the feature vector (characteristic quantity) to be used, which, in the context of this study, is the PSD (output–only) or modulus of the FRF (input–output) at n selected frequencies. Namely:

$$\text{PSD based version (output–only)} \quad \boldsymbol{\theta} = [S_{yy}(\omega_1), \ldots, S_{yy}(\omega_n)]^T, \tag{4a}$$

$$\text{FRF based version (input–output)} \quad \boldsymbol{\theta} = [|H(j\omega_1)|, \ldots, |H(j\omega_n)|]^T. \tag{4b}$$

As with all statistical time series methods for SHM [18], the damage detection methodology consists of two distinct phases: *Baseline* and *Inspection*. In the baseline phase the PSD (respectively FRF) (which includes the dynamics of the structure) in the healthy *and* damage states is obtained. In standard vibration based methodologies this is done using a single representative signal for each considered state. This selection is crucial for the correct performance of the method, and the conditions under which this signal is acquired may be decisive as well. Small changes in the environment, or a non–representative signal, may lead to inferior performance. In order to overcome these difficulties, an approach in which *multiple* signals (under different conditions) are considered in the baseline phase is adopted. In the inspection phase, given a new signal from an unknown state of the structure and in unknown environmental conditions, the method uses hypothesis testing to decide whether it is coming from the healthy or a damaged state of the structure. The two phases are described in more detail in the sequel.

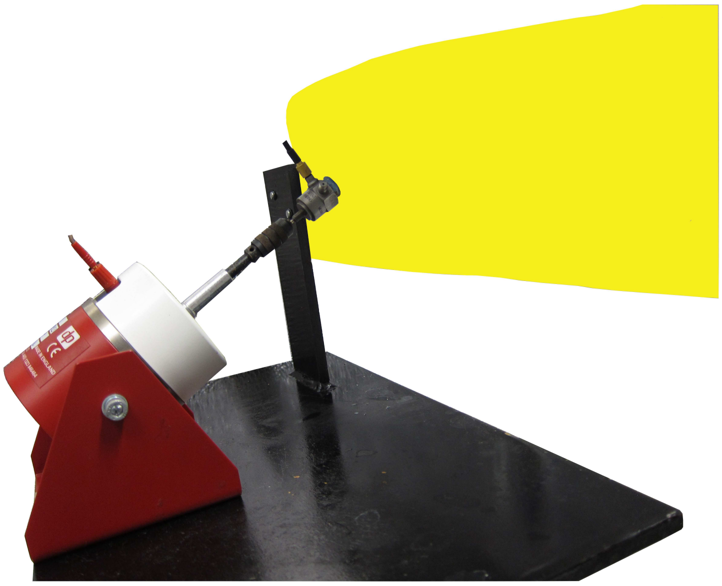

Figure 3: Detail of the experimental set-up.

3.1 Baseline phase

By means of using Principal Component Analysis (PCA) [19, pp. 1-6] a (vector) characteristic quantity (feature) insensitive to environmental changes, but still sensitive to the presence of damage, is sought. The procedure works as follows:

- *Step 1. Estimation of the feature covariance matrix.* A set of ρ_0 $n-$dimensional feature vectors $\boldsymbol{\theta} \in \Theta_0$ is used for the estimation of the covariance matrix. The features are obtained from different "healthy" data records under different environmental conditions. The sample mean $\overline{\boldsymbol{\theta}}$ over all healthy data is then obtained:

$$\overline{\boldsymbol{\theta}} = \frac{1}{\rho_0} \sum_{\boldsymbol{\theta} \in \Theta_0} \boldsymbol{\theta}, \tag{5}$$

along with the sample covariance matrix:

$$\widehat{\mathbf{P}} = \frac{\sum_{\boldsymbol{\theta} \in \Theta_0} (\boldsymbol{\theta} - \overline{\boldsymbol{\theta}})(\boldsymbol{\theta} - \overline{\boldsymbol{\theta}})^T}{\rho_0 - 1} \in \mathbb{R}^{n \times n}. \tag{6}$$

It should be noted that for the proper estimation of the covariance matrix the feature vector dimensionality n should be sufficiently smaller than the number ρ_0 of data records. When this is not the case, the empirical covariance estimate is potentially ill–conditioned, and thus non–invertible. In such cases alternative estimators, such as a shrinkage–based covariance estimator (which is always well conditioned and optimum in the mean square error sense) or a pseudomodel–based estimator may be used [20, 21].

- *Step 2. Principal Component Analysis.* The estimated covariance matrix is now decomposed using PCA as follows:

$$\widehat{\mathbf{P}} = \mathbf{U} \cdot \boldsymbol{\Lambda} \cdot \mathbf{U}^T, \tag{7}$$

where

$$\boldsymbol{\Lambda} = \mathrm{diag}\,(\lambda_1, \ldots, \lambda_n) \in \mathbb{R}^{n \times n}, \qquad \mathbf{U} = [\mathbf{u}_1 \ \ \ldots \ \ \mathbf{u}_n] \in \mathbb{R}^{n \times n}, \tag{8}$$

with diag$(\ldots)$ designating a diagonal matrix composed of the indicated elements, $\lambda_i (> 0)$ the $i-$th eigenvalue of $\widehat{\mathbf{P}}$ ordered in descendent order, and $\mathbf{u}_i$ the corresponding normalized eigenvector with $i = 1, \ldots, n$.

The transformation into principal components for any feature vector $\boldsymbol{\theta}$ is performed as:

$$\mathbf{s} = \mathbf{U}^T(\boldsymbol{\theta} - \overline{\boldsymbol{\theta}}) \in \mathbb{R}^n \tag{9}$$

which for elements in Θ_0 warrants a sample mean of $\mathbf{0}$, and diagonal covariance matrix $\boldsymbol{\Lambda}$.

- *Step 3. Dimensionality reduction.* The aim is to define a set of Principal Components in which damage detection is clear, irrespectively of the environmental conditions. Since in the construction of the covariance matrix different environmental conditions are accounted for, the majority of the variance in the feature vector is expected to come from the variation of those conditions. For this reason the "last" principal components (corresponding to the smallest eigenvalues) are expected to be less dependent on the environmental conditions, but, hopefully, still sensitive to damage. The general idea is then to *discard* the *first* $\underline{n}$ components, and from the remaining ones select a set of n_0 components that collectively provide sufficient sensitivity to damage, see Figure 4. For the selection of the specific components, in addition to the set Θ_0 (used for the estimation of the covariance matrix), a second set Θ_d consisting of ρ_d feature vectors from damaged structural states, under different environmental conditions, is used. This is needed in order to evaluate the damage detection capability of the different scalar components. The components to be finally retained are those that offer the best damage detection capability. The selected mathematical tool to measure this capability is the squared Mahalanobis distance[1] (Matlab function *mahal.m*). The reference set, with respect to which the Mahalanobis distance is computed, is that of the transformed feature vectors in Θ_0. Due to the definition of the principal components, this set is characterized by sample mean $\boldsymbol{\mu} = \mathbf{0}$ and diagonal covariance matrix, with elements λ_i, corresponding to the selected components in each case.

  The aim is to retain components for which the Mahalanobis distance is large when the feature vector belongs to a damaged structural state, but small when it corresponds to a healthy state. In Figure 5 an example involving three principal components is shown with sets Θ_0 (represented by the blue triangles) and Θ_d (represented by red circles). The blue set is the reference set with respect to which all distances are measured. The red circles represent damage cases. The distances of all blue dots and all red dots with respect to the set of blue dots are computed. It is seen how the blue triangles are centered around the zero vector. The Θ_d set is not completely separated from the Θ_0 one, but actually surrounding it. The aim is to retain the components which make these two sets as *separable* as possible (blue set as close to the $\mathbf{0}$ $j-$dimensional vector, and red set as separated as possible, leaving in general the blue set inside it). The inclusion of a new component should imply a better separation of the two sets.

s_1	s_2	...	$s_{\underline{n}}$	$s_{\underline{n}+1}$	...	s_n

DISCARD $\Leftarrow$ ‖ $\Rightarrow$ KEEP and work from the right end to select n_0 components

Figure 4: The elements of transformed feature vector $\mathbf{s}$ in relation to dimensionality reduction.

The indexes of the selected components are denoted by $b(1), \dots, b(n_0)$.

Once a feature vector $\boldsymbol{\theta}$ is given, its transformation into principal components is computed by means of equation (9). In the following when writing $D_j^2(\boldsymbol{\theta})$ the squared Mahalanobis distance is meant in the transformed principal component space using the j components characterized by indexes $b(1), \dots, b(j)$.

The specific substeps are as follows:

  - *Step 3a: Selection of* $\underline{n}$. A threshold is defined by $0 < \delta < 1$, and $\underline{n}$ is chosen as the minimum value for which:

[1] Formally the Mahalanobis distance of a multivariate vector $\mathbf{x} = [x_1, \dots, x_n]^T$ from a group of values with mean $\boldsymbol{\mu} = [\mu_1, \dots, \mu_n]^T$ and covariance matrix $\mathbf{S}$ is defined as [19, p. 237]

$$D(\mathbf{x}) = \sqrt{(\mathbf{x} - \boldsymbol{\mu})^T \mathbf{S}^{-1} (\mathbf{x} - \boldsymbol{\mu})}.$$

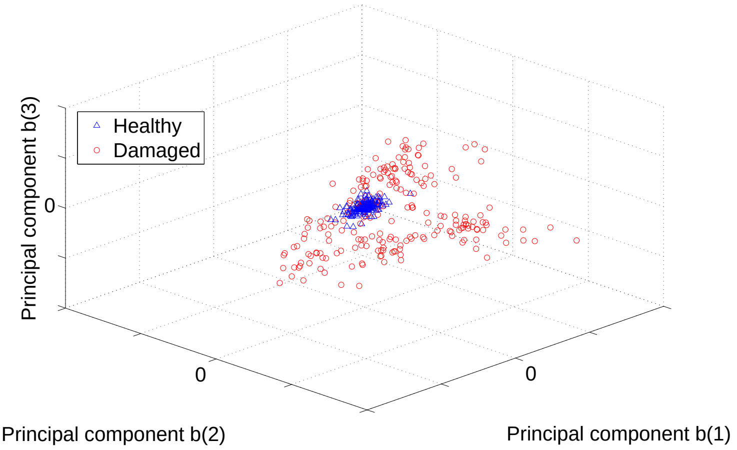

Figure 5: An example of 3–dimenional (three principal components) sets Θ_0 and Θ_d.

$$\frac{\sum_{j=1}^{\underline{n}} \lambda_j}{\sum_{j=1}^{n} \lambda_j} \geq \delta, \tag{10}$$

The first $\underline{n}$ components are the discarded, and certain, specifically n_0 components are to be kept among the set $\{s_{\underline{n}+1}, \ldots, s_n\}$, see Figure 4.

– *Step 3b: Selection of n_0 and specific components.* This is an iterative step in which the introduction of a new component is tested and accepted in case an improvement on the separability of sets Θ_0 and Θ_d is achieved. At step j, with $j = 1, \ldots, n - \underline{n}$, the inclusion of any component not previously included is checked. In principle all the components are to be tested, even if really the process stops after the selection of n_0, so at $j = n_0 + 1$, when the addition of a new component will no longer involve an improvement in the separability of the two sets, as will be shown in the sequel. For this process the following ratio is computed:

$$R_j = \frac{\min_{\boldsymbol{\theta} \in \Theta_d} D_j^2(\boldsymbol{\theta})}{\max_{\boldsymbol{\theta} \in \Theta_0} D_j^2(\boldsymbol{\theta})} \tag{11}$$

where D_j^2 denotes the squared Mahalanobis distance with respect to the set Θ_0, with the subindex indicating the dimension of the space in which the distance is being computed ($\mathbb{R}^j$). This quotient measures the ratio between the minimum Mahalanobis distance of all the “damaged” baseline data records (the minimum is taken to consider the most difficult damage to be detected) with respect to the set Θ_0 and the maximum distance of the “healthy” ones to the same set (the maximum is taken as this would be the most probable false alarm). Namely this distance is given by:

$$D_j^2 = \mathbf{s}_j^T \boldsymbol{\Lambda}_j^{-1} \mathbf{s}_j, \tag{12}$$

with

$$\begin{gathered} \mathbf{s}_j = \mathbf{U}_j^T (\boldsymbol{\theta} - \overline{\boldsymbol{\theta}}) \in \mathbb{R}^j, \qquad \boldsymbol{\Lambda}_j = \operatorname{diag}\left(\lambda_{b(1)}, \ldots, \lambda_{b(j)}\right) \in \mathbb{R}^{j \times j}, \\ \mathbf{U}_j = \left[\mathbf{u}_{b(1)} \; \cdots \; \mathbf{u}_{b(j)}\right] \in \mathbb{R}^{n \times j}. \end{gathered} \tag{13}$$

In the case $j = 1$, $b(1)$ is selected as the index that maximizes the set:

$$\{R_1, \; b(1) = \underline{n} + 1, \ldots, n\}. \tag{14}$$

Once $b(1)$ is selected and its corresponding ratio $R_1^{\max}$ computed, for each successive $j = 2, \ldots, n_0 + 1$ the set:

$$\{R_j, \; b(j) = \underline{n} + 1, \ldots, n, \; b(j) \neq b(k), \; \forall k < j\}. \tag{15}$$

is maximized, $b(j)$ is the index corresponding to this maximum $R_j^{\max}$.

The process is then repeated until $R_j^{\max} = R_{j-1}^{\max}$. In this moment $n_0 = j-1$ (the first value for which the maximum is achieved), and the maximum separability for the training sets Θ_0 and Θ_d has been obtained.

So, finally n_0 components are retained and the matrix:

$$\mathbf{U}_{n_0} = \left[\mathbf{u}_{b(1)} \ \dots \ \mathbf{u}_{b(n_0)}\right] \in \mathbb{R}^{n \times n_0}, \tag{16}$$

is used for transformation of new feature vectors by means of:

$$\mathbf{s}_{n_0} = \mathbf{U}_{n_0}^T (\boldsymbol{\theta} - \overline{\boldsymbol{\theta}}) \in \mathbb{R}^{n_0}. \tag{17}$$

3.2 Inspection phase

In the inspection phase given a new feature vector $\boldsymbol{\theta}_u$ from an unknown state, the transformation of equation (17) with $\boldsymbol{\theta} = \boldsymbol{\theta}_u$ is done so $\mathbf{s}_{n_0} \in \mathbb{R}^{n_0}$ is computed (using $\overline{\boldsymbol{\theta}}$ from the baseline phase) and the squared Mahalanobis distance:

$$D_{n_0}^2 = \mathbf{s}_{n_0}^T \boldsymbol{\Lambda}_{n_0}^{-1} \mathbf{s}_{n_0}, \text{ with } \boldsymbol{\Lambda}_{n_0} = \operatorname{diag}\left(\lambda_{b(1)}, \dots, \lambda_{b(n_0)}\right) \in \mathbb{R}^{n_0 \times n_0} \tag{18}$$

is computed.

In a general context, by applying the central limit theorem, since each principal component is a linear combination of random variables, normality may be assumed, even if the original variables are not normally distributed (see [19, p. 236]). Taking this fact into account, the squared Mahalanobis distance in (18) is is a sum of n_0 squared $N(0,1)$ and mutually independent random variables, so the distribution followed by D^2 is χ^2 with degrees of freedom given by the number of principal components retained in the process, namely n_0.

Thus the hypothesis testing problem may be set up as:

$$\begin{array}{lcll} H_o & : & D_{n_0}^2(\boldsymbol{\theta}_u) = 0 & \text{(null hypothesis – healthy structure)} \\ H_1 & : & \text{Else} & \text{(alternative hypothesis – damaged structure).} \end{array} \tag{19}$$

Taking into account that $D_{n_0}^2 \sim \chi^2(n_0)$, then for a selected α risk level (false alarm probability equal to α), the quantity $D_{n_0}^2(\boldsymbol{\theta}_u)$ should be in the range $(0, \chi_{1-\alpha}^2(n_0)]$ with probability $1-\alpha$, so the hypothesis test is:

$$\begin{array}{ccc} D_{n_0}^2(\boldsymbol{\theta}_u) \leq \chi_{1-\alpha}^2(n_0) & \Rightarrow & \text{Healthy structure} \\ \text{Else} & \Rightarrow & \text{Damaged structure.} \end{array} \tag{20}$$

where $\chi_{1-\alpha}^2(n_0)$ denotes the critical point of the χ^2 distribution with n_0 degrees of freedom at level $1-\alpha$.

4 Results

The methodology described in the previous section is now applied to the data, for two different considerations of the feature vector, as shown in equations (4a)–(4b). The results for the two versions are considered in two different subsections. All the detailed results presented are based in output location Y2.

First, Welch based PSD and FRF estimates, obtained for long segments ($L = 2\,048$ samples, 0% overlap, $K = 16$ averaged segments) are depicted for output Y2 in Figures 6 and 7. The estimates are shown along with their 95% confidence intervals (note that the confidence intervals are narrower for the FRF than for the PSD).

In Figures 6(a) and 7(a) the PSD and FRF, respectively, interval estimates for two "healthy" signals at two different temperatures are shown, whereas in Figures 6(b) and 7(b) those of a healthy and a "damaged" signal at the same temperature are shown. It is seen that changes in the PSD or FRF and interval estimate due to temperature difference (even if it is just 4°C) are larger than those due to damage at a fixed temperature (especially at high frequencies). This is a problem in standard methodologies, since they do not usually account for environmental effects. With the present methodology a baseline reference that attempts to account for these uncertainties is employed, so that damage detection may be performed irrespectively of the specific environmental conditions under which the current signal has been acquired.

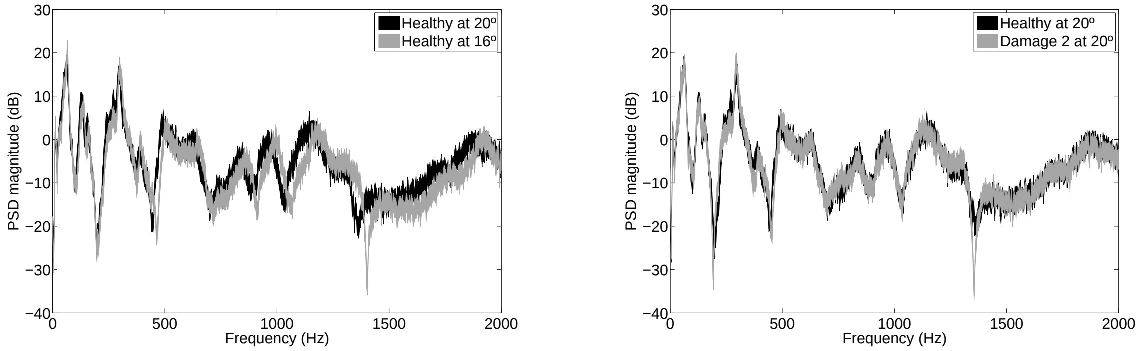

(a) (b)

Figure 6: Preliminary results: PSD estimates along with 95% confidence intervals for the vibration response position Y2: (a) healthy case at 20°C (black region) compared with healthy case at 16°C (grey region), (b) healthy case at 20°C (black region) compared with damage 2 at the same temperature of 20°C (grey region).

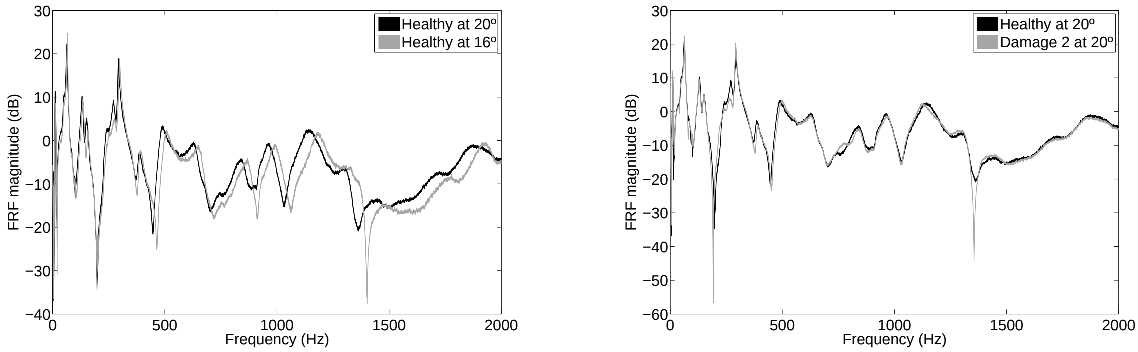

(a) (b)

Figure 7: Preliminary results: FRF estimates along with 95% confidence intervals for the vibration response signal position Y2: (a) healthy case at 20°C (black region) compared with healthy case at 16°C (grey region), (b) healthy case at 20°C (black region) compared with damage 2 at the same temperature of 20°C (grey region).

The specific values of the methodology are chosen as in Table 2. For good estimation of the covariance matrix it is desirable to have more data records than parameters to estimate. For this reason PSD and FRF estimation is based on a short segment length ($L = 128$). This, for positive frequencies only, gives rise to a feature vector of length of 65 considering frequencies to 2 560 Hz ($f_s = 5\ 120\ Hz$). Since the excitation range has only been up to 2 000 Hz, the feature vector to be used is limited to a dimensionality of $n = 51$.

The set Θ_0 is then composed of 5 data records per structural condition (baseline phase; Table 1) from all available healthy conditions, which gives a dimension for this set of $\rho_0 = 160$. Analogously for Θ_d, 5 data records from each structural condition are used, resulting in $\rho_d = 215$ (Table 1). The values of $\underline{n}$ and n_0 shown in Table 2 are the ones corresponding to the PSD and FRF based versions in sensor position Y2. All of the other parameters above, including δ and α, are kept common for all response (sensor) positions and both PSD and FRF versions.

All positions have been analyzed with both versions of the methodology, and overall performance results are provided in Table 3, where the two types of considered damages are distinguished. It is interesting that the larger damage (D2) is slightly less detectable than the smaller one (D1). Although the precise reasons for this are unclear, it may be related to the fact that – unlike with D1 – two cases (implying more variability) are associated with D2: water sprayed and not sprayed (see Table 1).

Estimation method	Welch	ρ_0	160 (from 32 different conditions)
Window type	Hamming	ρ_d	215 (from 43 different conditions)
L	128 samples	$\underline{n}$	PSD version: 11
Overlap	0 samples		FRF version: 18
K	256	n_0	PSD version: 12
n	51		FRF version: 13
δ	0.997	α	10^{-10}

Table 2: Estimation details and specific values of parameters.

Method	*Sensor*	*False alarms*	*False alarm rate*	*Undetected damages*		*Detection rate*	
				D1	D2	D1	D2
PSD Based version	1	2/1 120	0.2%	0/385	13/1 120	100.0%	98.8%
	2	15/1 120	1.3%	1/385	12/1 120	99.7%	98.9%
	3	7/1 120	0.6%	4/385	22/1 120	99.0%	98.0%
	4	12/1 120	1.1%	0/385	0/1 120	100.0%	100.0%
FRF Based version	1	5/1 120	0.5%	0/385	35/1 120	100.0%	96.9%
	2	5/1 120	0.5%	1/385	14/1 120	99.7%	98.8%
	3	3/1 120	0.3%	0/385	0/1 120	100.0%	100.0%
	4	1/1 120	0.1%	0/385	0/1 120	100.0%	100.0%

Table 3: Detailed SHM results for each sensor position distinguishing the two versions (PSD and FRF) and the two levels of damage severity (inspection data records only).

4.1 PSD based version results

To make the procedure clearer, let us show some intermediate results step by step for the second output. The corresponding ones for the FRF based version are shown in the next subsection.

- *Step 1:* The 160 healthy data sets are used to compute the covariance matrix as indicated in Equation (6).
- *Step 2:* PCA is performed in the previously computed covariance matrix by means of the Matlab function *princomp.m*.
- *Step 3:*
  - *Step 3a:* The value obtained for $\underline{n}$ is 11, so this means that the first 11 principal components explain the 99.7% of the variance present in the PSD. This is represented in Figure 8 (blue continuous line).
  - *Step 3b:* Now an iterative process starts leading to the selection of the n_0 components. The 160 “healthy” data records, along with the 215 “damaged” data records are used in this baseline phase (Table 1). In Figure 9(a) just the first selected component behavior is shown, a great improvement is achieved with the inclusion of the second component 9(b). The main objective is to maximize the distance between the “healthy” data records and the “damaged” ones. In Figure 9(c) an intermediate step is shown and in Figure 9(d) the final selection is shown with the data records considered in the baseline phase. In this case it may be seen that now all “healthy” data records have distances lower than the “damaged” data records, which is the desirable behavior. Note that in all subfigures of Figure 9, “healthy” data records are indicated in blue, whereas damaged data sets are red (damage 1) or green (damage 2). These three groups are separated by dashed vertical lines. Data records are ordered in descendent order of temperature. Also dotted vertical lines are included in the healthy and damage 2 cases to distinguish the cases without water sprayed from the ones in which water has been sprayed. The maximum distance from “healthy” data records and the minimum from the “damaged” ones is color filled since this are the values used in the computation of each R_j. In Figure 10(a), the R_j ratios are shown for a few iterations. On the horizontal axis $n - \underline{n} = 40$ (from

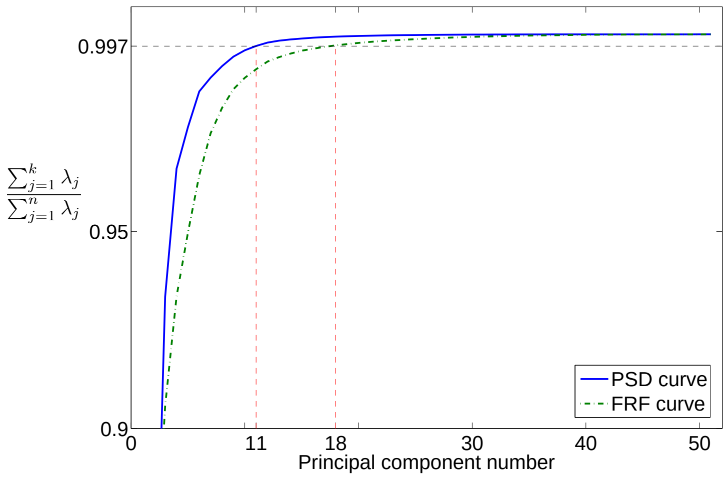

Figure 8: Baseline phase: Determination of $\underline{n}$ in the PSD and FRF based versions. The principal component number is shown on the horizontal axis, and the fraction of variance cumulatively explained by the considered component is depicted by the curve (blue solid line for the PSD based version and green dashed line for the FRF one). The selected δ and the obtained $\underline{n}$ are indicated by the horizontal and vertical dashed lines, respectively.

the 12$^{\text{th}}$ until the 51$^{\text{st}}$) components are analyzed. Since the selected number of components is 12, only 12 iterations are done (then $R_{13}^{\max} = R_{12}^{\max}$) the cases $j = 1, 5, 10, 12$ are shown. The selected components are marked with a solid blue circle.

In Figure 12(a) the final damage detection results with the selected principal components are shown in the PSD based version for data records from the inspection phase (which are different from those used in the baseline phase – cross–validation principle; Table 1). The first 1 120 data records are healthy time series (35 for every temperature available with and without water), with 735 without water and the next 385 with water; the next 1 505 data records correspond to damaged cases (also 35 data sets for every damage at specific temperatures and with water sprayed when available), so the first 385 correspond to damage 1, the next 735 to damage 2 without water and the last 385 to damage 2 with water prayed. Healthy, damage 1 and damage 2 cases are separated by dashed vertical lines, the difference between water sprayed and not sprayed is made by a dotted line for the healthy and damaged 2 cases. In the y axis the squared Mahalanobis distance is represented. A total number of 15 false alarms and 13 undetected damage is obtained (1 from damage 1 and 12 from damage 2).

4.2 FRF based version results

The steps are exactly as before, so not all the written details are repeated here.

Step 3a for this case is also shown in Figure 8 (green dashed line). In this case the value obtained for $\underline{n}$ is 18 (much bigger than before) so this means that the first 18 principal components explain the 99.7% of the variance present in the FRF. So with respect to the PSD based version more components are needed to explain the same amount of variance.

Figure 11 is the equivalent to the previously presented 9. For this case the value obtained for n_0 is 13 (one more than before). Now, in Figure 10(b) the cases $j = 1, 5, 10, 13$ are shown. Again for the baseline data records a perfect separation of both sets is achieved with the final selection of components. The separation was better in the PSD based version for the baseline data records as can be seen by the higher value of R_j obtained in Figure 10(a) with respect to the one obtained in 10(b). This can also be observed by comparing 9(d) with 11(d).

In Figure 12(b) the final damage detection results with the selected principal components are shown for the FRF based version for data records from the inspection phase. Comments made in the previous subsection regarding the description of the figure are again valid here. In this case a total number of 5 false alarms and 15 undetected damages are obtained (1 from damage 1 and 14 from damage 2). The number of false alarms has been quite significantly reduced even if the undetected damages has slightly increased.

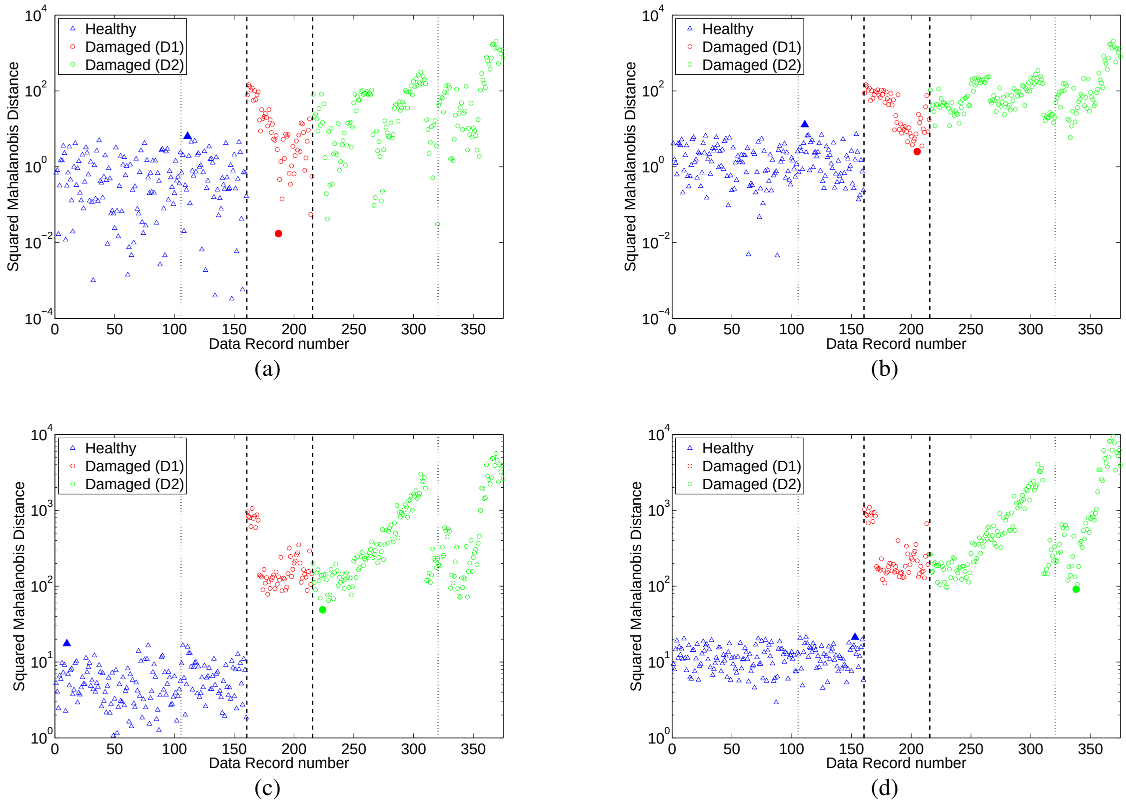

Figure 9: PSD based version. Baseline phase (pictorial representation of Step 3 in selecting the principal components to be included): Squared Mahalanobis distance from the various ("healthy" and "damaged") data records to the "healthy" set. The first 160 data sets (blue triangles) correspond to the healthy blade (the first 105 without water sprayed, the next 55 with water sprayed, separated by dotted vertical lines). The next 55 (red circles) correspond to damage 1 and the last 160 (green circles) to damage 2 (also here the first 105 without water sprayed, the next 55 with water sprayed, separated by dotted vertical lines). The three main groups are distinguished by dashed vertical lines. The maximum distance among all "healthy" data records is designated by a solid blue triangle. The minimum distance among all "damaged" data records is designated by a solid red or green circle. (a) One principal component included, (b) two principal components included, (c) intermediate step with six principal components included, (d) final selection of $n_0 = 12$ principal components.

4.3 General remarks

Making the comparison between PSD (output–only) and FRF (input–output) based versions of the methodology, it is seen that the results are quite comparable. Overall, it can be said that the FRF based version performs slightly better, as could be expected since more information is being used, but the improvement is not really significant. Regarding the false alarms, all the values are under 0.5% for the FRF based version, whereas in the PSD one some values are over 1%. With respect to undetected damages the FRF based version presents more cases in which a 100% of success is achieved, even if for two of the outputs, there is an increase in the number of undetected damages (from damage 2) with respect to the PSD based version.

5 Conclusions

A vibration–based statistical time series type damage detection methodology, capable of operating under varying environmental and operational conditions, has been postulated based on Power Spectral Density (PSD) (output–only) and FRF (input–output) estimation and Principal Component Analysis (PCA). Detection is based on principal components selected to be independent of environmental conditions, but still sensitive to damage. The methodology is characterized by conceptual and computational simplicity. Its application to damage de-

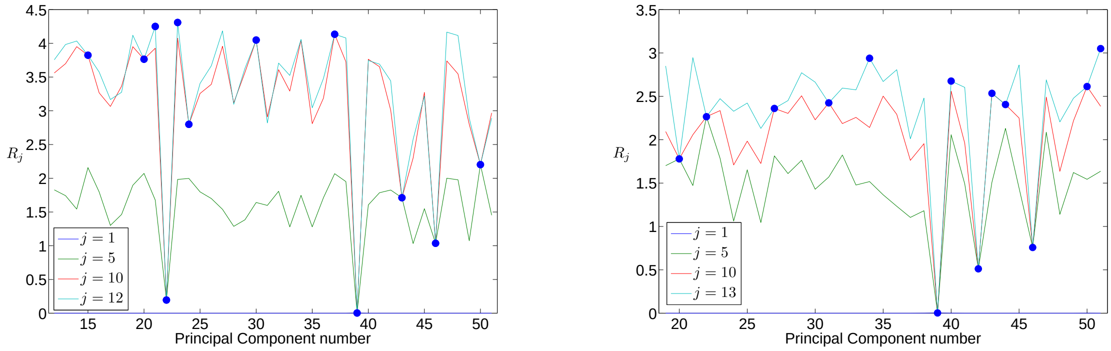

(a) (b)

Figure 10: Baseline Phase: The ratio R_j computed for different iterations of addition of a new principal component. The blue solid circles designate the principal component chosen for maximizing the ratio R_j at each step. (a) PSD based version, (b) FRF based version.

tection in a laboratory-scale wind turbine blade, subject to two levels of damage and varying conditions that include sprayed water (simulating rain) and temperatures in the range $[-20, 20]$°C, has been demonstrated using a single vibration acceleration response. The methodology proved effective, exhibiting a detection rate of over 99% for damage 1 and over 96% for damage 2 and a corresponding false alarm rate below 2% in all cases. The performance of the FRF based version (input–output) is slightly better than the PSD one (output–only) even if the improvement cannot be considered very significant.

The presented methodology will be next applied on a Finite Element model of a real full size wind turbine blade, under different environmental conditions.

Acknowledgement

The support of this work by the EU FP7 ITN project SYSWIND (Grant 238325) is gratefully acknowledged.

References

[1] H. Sohn, *Effects of environmental and operational variability on structural health monitoring*, in Philosophical Transactions of the Royal Society A: Physical and Engineering Sciences, Vol. 356, The Royal Society (2007), pp.539-560.

[2] J.T. Kim, J.H. Park, B.J. Lee, *Vibration-based damage monitoring in model plate-girder bridges under uncertain temperature conditions*, Engineering Structures, Vol. 29, No. 7, Elsevier (2007), pp. 1354-1365.

[3] B. Peeters, G. De Roeck, *One-year monitoring of the Z24-bridge: environmental effects versus damage events*, Earthquake Engineering and Structural Dynamics, Vol. 30, No. 2, John Wiley & Sons (2001), pp. 149-171.

[4] H. Sohn, M. Dzwonczyk, E.G. Straser, A.S. Kiremidjian, K.H. Law, T. Meng, *An experimental study of temperature effect on modal parameters of the Alamosa Canyon Bridge*, Earthquake Engineering and Structural Dynamics, Vol. 28, No. 8, John Wiley & Sons (1999), pp. 879-897.

[5] K. Worden, H. Sohn, C.R. Farrar, *Novelty detection in a changing environment: Regression and interpolation approaches*, Journal of Sound and Vibration, Vol. 258, No. 4, University Press (2002), pp. 741-761.

[6] P. Kraemer, *Schadensdiagnoseverfahren fur die Zustandsuberwachung von Offshore-Windenergieanlagen*, PhD Thesis, Siegen, 2011.

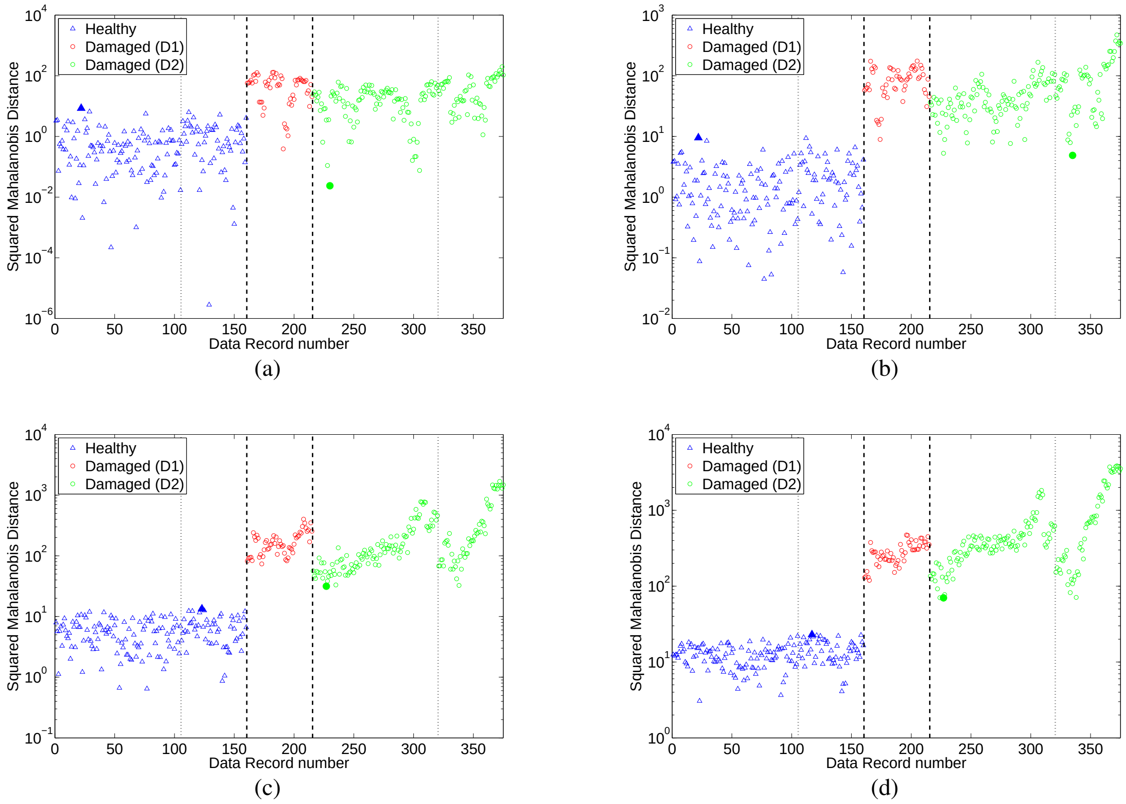

Figure 11: FRF based version. Baseline phase (pictorial representation of Step 3 in selecting the principal components to be included): Squared Mahalanobis distance from the various (“healthy” and “damaged”) data records to the “healthy” set. The first 160 data sets (blue triangles) correspond to the healthy blade (the first 105 without water sprayed, the next 55 with water sprayed, separated by dotted vertical lines). The next 55 (red circles) correspond to damage 1 and the last 160 (green circles) to damage 2 (also here the first 105 without water sprayed, the next 55 with water sprayed, separated by dotted vertical lines). The three main groups are distinguished by dashed vertical lines. The maximum distance among all “healthy” data records is designated by a solid blue triangle. The minimum distance among all “damaged” data records is designated by a solid red or green circle. (a) One principal component included, (b) two principal components included, (c) intermediate step with six principal components included, (d) final selection of $n_0 = 13$ principal components.

[7] J.D. Hios, S.D. Fassois, *Stochastic identification of temperature effects on the dynamics of a smart composite beam: assessment of multi-model and global model approaches*, Smart Materials and Structures, Vol. 18, No. 3, IOP Publishing (2009), 035011 (15pp).

[8] G. Manson, B.C. Lee, W.J. Staszewski, *Eliminating environmental effects from Lamb wave-based structural health monitoring*, in *Proceedings of the International Conference on Noise and Vibration Energy (ISMA), 2004 September 20-22*, Leuven (2004), pp. 471-484.

[9] A.-M. Yan, G. Kerschen, P. De Boe, J.-C. Golinval, *Structural damage diagnosis under varying environmental conditions – Part I: A linear analysis*, Mechanical Systems and Signal Processing, Vol. 19, No. 4, Elsevier (2005), pp. 847-864.

[10] A. Deraemaeker, E. Reynders, G. De Roeck, J. Kullaa, *Vibration-based structural health monitoring using output-only measurements under changing environment*, Mechanical Systems and Signal Processing, Vol. 22, No. 1, Elsevier (2008), pp. 34-56.

[11] É. Balmès, M. Basseville, F. Bourquin, L. Mevel, H. Nasser, F. Treyssède, *Merging sensor data from multiple temperature scenarios for vibration monitoring of civil structures*, Structural Health Monitoring, Vol. 7, No. 2, SAGE Publications (2008), pp. 129-142.

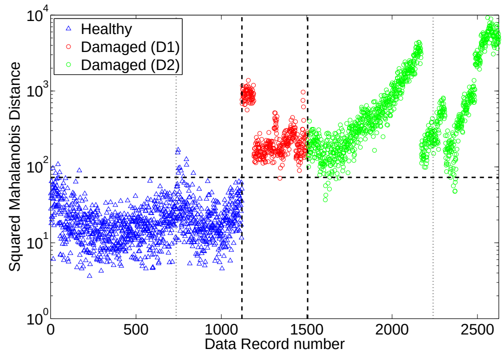

(a)

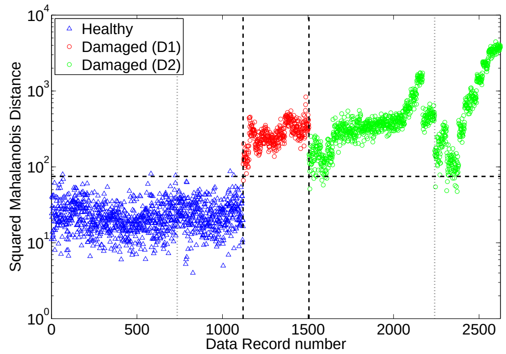

(b)

Figure 12: Inspection Phase: Damage detection results for data records from the inspection phase based on sensor position Y2 (false alarm probability $\alpha = 10^{-10}$). The first 1 120 data records (blue triangles) correspond to the healthy condition, the next 385 record (red circles) correspond to damage 1, whereas the remaining 1 120 records (green circles) correspond to damage 2. Dashed vertical lines distinguish the three different conditions, whereas dotted vertical lines separate the data records without water sprayed (first 735) from the ones with water sprayed (next 385). The threshold corresponding to the selected α is designated by the dashed horizontal line. (a) PSD based version with $n_0 = 12$ principal components, (b) FRF based version with $n_0 = 13$ principal components.

[12] E.J. Cross, K. Worden, Q. Chen. *Cointegration: a novel approach for the removal of environmental trends in structural health monitoring data*, in *Proceedings of the Royal Society A: Mathematical, Physical and Engineering Science, 2011 September*, Vol. 467, No. 2133, The Royal Society (2011), pp. 2712-2732.

[13] A. Light-Marquez, A. Sobin, G. Park, K. Farinholt, *Structural Damage Identification in Wind Turbine Blades Using Piezoelectric Active Sensing*, Structural Dynamics and Renewable Energy, Vol. 1, Springer (2011), pp. 55-65.

[14] A. Ghoshal, M.J. Sundaresan, M.J. Schulz, P. Frank Pai, *Structural health monitoring techniques for wind turbine blades*, Journal of Wind Engineering and Industrial Aerodynamics, Vol. 85, No. 2, Elsevier (2000), pp. 309-324.

[15] S.N. Ganeriwala, V. Kanakasabai, and M. Richardson, *Modes indicate cracks in wind turbine blades. Rotating Machinery*, Rotating Machinery, Structural Health Monitoring, Shock and Vibration, Vol. 5, Springer (2011), pp. 509-513.

[16] M.A. Rumsey, J.A. Paquette, *Structural health monitoring of wind turbine blades*, in *Proceeding of The 15th International Symposium on: Smart Structures and Materials & Nondestructive Evaluation and Health Monitoring, 2008 March 9–13*, San Diego (2008), pp. 69330E.

[17] A. Gómez González, S.D. Fassois, *Vibration–response–based damage detection for scale wind turbine blades under varying environmental conditions*, in *Proceedings of the Conference on Wind Energy Science and Technology, 2013 October 3–4*, Ankara (2013).

[18] S.D. Fassois, J.S. Sakellariou, *Statistical Time Series Methods for SHM*, Encyclopedia of Structural Health Monitoring, Wiley Online Library (2009), pp. 443-472.

[19] I. Jolliffe, *Principal Component Analysis*, Wiley Online Library (2005).

[20] J. Schäfer, K. Strimmer, *A shrinkage approach to large-scale covariance matrix estimation and implications for functional genomics*, Statistical Applications in Genetics and Molecular Biology, Vol. 4, No. 1(article 32), de Gruyter (2005), pp. 1175-1189.

Acronym/Parameter name	*Description*
PCA	Principal Component Analysis
PSD	Power Spectral Density
CPSD	Cross Power Spectral Density
FRF	Frequency Response Function
N	Signal (time series) length
L	Segment length in Welch based PSD or FRF estimation
K	Number of non–overlapping segments in Welch based PSD or FRF estimation
$\boldsymbol{\theta}$	Feature vector (characteristic quantity) used in the PCA
n	Feature vector length
Θ_0	Set of "healthy" data records used in the baseline phase
ρ_0	Dimension of set Θ_0
Θ_d	Set of "damaged" data records used in the baseline phase
ρ_d	Dimension of set Θ_d
δ	Value between 0 and 1 (see next item)
$\underline{n}$	Number of components explaining the $\delta \times 100\%$ of the variance
n_0	Selected number of principal components used in detection
α	Critical value for the hypothesis test

Table 4: Acronyms and symbols

[21] P.G. Michaelides, S.D. Fassois, *Uncertain Structural Dynamics Identification via a Random Coefficient ARX Model Based Method*, in *Proceedings of the USD International Conference on Uncertainty in Structural Dynamics, 2012 September 17-19*, Leuven (2012), pp. 5025-5038.

A Appendix

- Important conventions and symbols.

  Bold–face upper/lower case symbols designate matrix/column–vector quantities, respectively. Matrix transposition is indicated by the superscript ^{T}.

  A functional argument in brackets designates function of an integer variable; for instance $x[t]$ is a function of normalized discrete time $(t = 1, 2, \ldots)$. A functional argument including the imaginary unit designates complex function; for instance $X(j\omega)$ is a complex function of ω.

  A hat designates estimator/estimate of the indicated quantity; for instance $\widehat{\boldsymbol{\theta}}$ is an estimator/estimate of $\boldsymbol{\theta}$.

  The subscripts 'o', 'd', and 'u' designate quantities associated with the nominal (healthy), damaged and current (unknown) state of the structure, respectively.

  Other acronyms and symbols used are shown in table 4.